



***SH* velocity and compositional models near the 660-km discontinuity beneath South America and northeast Asia**

Yi Wang,¹ Lianxing Wen,¹ Donald Weidner,¹ and Yumei He²

Received 25 May 2005; revised 22 March 2006; accepted 11 April 2006; published 25 July 2006.

[1] We constrain *SH* wave velocity structures near the 660-km discontinuity beneath South America and northeast Asia, using triplicated phases near the discontinuity recorded in the epicentral distance range of 10°–35° for three deep events. We then explore mineralogical and compositional models appropriate for explaining the inferred seismic structures between the two regions. *SH* velocity structures near the 660-km discontinuity are found to be different in the two regions. Beneath South America, the velocity gradient above the 660-km discontinuity is larger than that of Preliminary Earth Reference Model (PREM), while the velocity jump across the discontinuity is the same as PREM. Beneath northeast Asia, the velocity gradient above the 660-km discontinuity is the same as that of PREM, while the velocity jump across the discontinuity is larger than PREM. Both regions are characterized by a large velocity gradient extending about 80 km deep below the 660-km discontinuity. The different velocity structures require different mineralogical models in the transition zone in the two regions. The larger velocity gradient above the 660-km discontinuity beneath South America requires existence of the ilmenite phase in the bottom of transition zone, while that beneath northeast Asia can be explained by the temperature and pressure dependence of elastic properties of the major mantle mineral assemblages. The observed large velocity gradients in the top of the lower mantle can be explained by gradual transformation of garnet to perovskite persisting to greater depths. The velocity jump across the 660-km discontinuity beneath South America, in the presence of the ilmenite phase in the bottom of the transition zone, requires a bulk composition of more garnet than the pyrolite model, while a larger velocity jump across the discontinuity beneath northeast Asia requires a larger fraction of garnet transforming to perovskite across the discontinuity than what is required for explaining PREM. These different mineralogical models can be caused by different mantle temperature or composition, especially the aluminum content in mantle composition. The presence of garnet 80 km below the 660-km discontinuity in the two regions may be explained by a uniform composition in the lower mantle with an aluminum content of 3.4%. The existence of ilmenite in the bottom of the transition zone beneath South America and the absence of ilmenite beneath northeast Asia can be explained by either a difference in mantle temperature of about 100°C (with that beneath South America being lower) between the two regions assuming a uniform mantle composition or, alternatively, a difference in aluminum content of about 1% (with that beneath South America being lower) between the two regions without invoking a temperature difference between the two regions. We also discuss conditions of mantle composition and temperature that double discontinuities may occur near the 660-km depth, as well as the depth separation and velocity jumps of the double discontinuities. For the inferred mantle temperature and composition beneath South America and northeast Asia, the maximum separation of the double discontinuities is 20 km and cannot be resolved by the *SH* wave data.

Citation: Wang, Y., L. Wen, D. Weidner, and Y. He (2006), *SH* velocity and compositional models near the 660-km discontinuity beneath South America and northeast Asia, *J. Geophys. Res.*, *111*, B07305, doi:10.1029/2005JB003849.

¹Department of Geosciences, State University of New York at Stony Brook, Stony Brook, New York, USA.

²Institute of Geology and Geophysics, Chinese Academy of Sciences, Beijing, China.

1. Introduction

[2] Understanding mantle composition is important in many aspects of geophysics. For example, in large-scale modeling of the surface geodynamical observations, such as geoid, topography, and plate motions, predictions are usually made by assuming a three-dimensional instantaneous Newtonian flow, with density anomalies usually derived

from seismic tomographic models by applying velocity-density scalings [e.g., Hager, 1984; Richards and Hager, 1984; Morgan and Shearer, 1993; Wen and Anderson, 1997a, 1997b]. If mantle composition is known, the velocity-density scalings should represent a thermal and compositional indicator to the Earth's interior and serve as a link among geodynamics, seismology and mineral physics.

[3] Mantle composition is also important in understanding phase transformations in the mantle, and phase transformations are important in understanding mantle dynamics. For example, the endothermic phase transformation from ringwoodite to perovskite plus magnesiowustite may introduce temporary layering through the 660-km discontinuity [Honda and Balachandar, 1993; Tackley et al., 1993]. The seismically inferred transition zone thickness has often been used as a thermometer, assuming an endothermic phase transition at the 660-km discontinuity and an exothermic phase transition at the 410-km discontinuity. However, mantle composition consists of two major components: an olivine-normative component and a pyroxene-normative component. The properties of the phase transformations and the actual paths of these phase transformations are complex and strongly depend on mantle composition and chemical interaction between the subsystems in the composition. For example, the 660-km discontinuity is actually caused by at least two phase transformations: from garnet to perovskite and from ringwoodite to perovskite plus magnesiowustite [Akaogi and Akimoto, 1979; Ito and Takahashi, 1987; Irifune and Ringwood, 1987]. These two phase transformations have different characteristics. While the breakdown of ringwoodite is endothermic, the phase transformation from garnet to perovskite is likely exothermic. These two phase transformations can also interact chemically. The actual paths of the perovskite-forming processes strongly depend on mantle temperature and composition [Weidner and Wang, 2000].

[4] While the properties of these phase transformations depend on mantle composition and chemical interaction between the two subsystems in the mantle, they result in different seismic structures near the 660-km discontinuity and can be directly tested using seismic data. For example, the velocity gradient above the 660-km discontinuity is sensitive to the presence of ilmenite above the discontinuity. The velocity jump across the 660-km discontinuity is sensitive to the amount of garnet transforming to perovskite across the discontinuity. With increasing amount of experimental data, now we can quantitatively calculate velocity and density profiles based on different compositional models, so these compositional models can be directly constrained by seismic data.

[5] In this study, we use joint modeling of seismic and mineral physics data to study the seismic *SH* velocity structures and mineralogical models near the 660-km discontinuity beneath South America and northeast Asia. We adopt waveform modeling to constrain the seismic structure. Synthetics are calculated by the reflectivity programs [Zhu and Rivera, 2002]. We also explore the conditions of mantle composition and temperature that are appropriate for explaining the inferred mineralogical models between the two regions. We discuss seismic data in section 2, the shear wave velocity structures beneath South America and northeast Asia in sections 3 and 4, the compositional and

mineralogical models in the two regions in section 5, the possibility of double 660-km discontinuities in section 6, and comparisons with previous studies in section 7.

2. Seismic Data

[6] Our study regions are South America and northeast Asia (Figure 1). The velocity structures near the 660-km discontinuity are constrained using triplicated phases recorded in the epicentral distance range of 10° – 35° for a deep event occurring in South America subduction zone and two events occurring in northeast Asia (Table 1). In order to minimize the effects of lateral seismic heterogeneities on the seismic wave propagation, we either use the seismic data recorded in seismic arrays or check the consistency of results from the data sampling different directions. The South America event is selected from the seismic data recorded in two PASSCAL experiments (BANJO and BLSP) in South America for events occurring in the South America subduction zone from January 1994 to September 1995. Note that the seismic data sample the transition zone beneath South America in a small azimuthal range (Figure 1a). The two Asia events are selected from the data recorded at 48 broadband stations in the New Chinese Digital Seismic Network (NCDSN) for events occurring in northeast Asia from August 2001 to February 2004. The two events sample the transition zone in the directions approximately perpendicular to each other (Figure 1b). The signal to noise ratios of the seismic data for these three events are high. Our approach is similar to the seismic studies using triplication phases in the upper mantle distance ranges [e.g., Helmberger and Wiggins, 1971; Burdick and Helmberger, 1978; Given and Helmberger, 1980; Walck, 1984; Grand and Helmberger, 1984a; Grand and Helmberger, 1984b; LeFevre and Helmberger, 1989; Cummins et al., 1992; Neele, 1996; Brudzinski et al., 1997; Melbourne and Helmberger, 1998; Zhao et al., 1999; Brudzinski and Chen, 2000; Brudzinski and Chen, 2003; Chen and Brudzinski, 2003; Song et al., 2004]. In this study, we use deep events to avoid the effect of shallow velocity structures. For a shallow event, the triplications from other shallow discontinuities (e.g., the 410-km discontinuity) will also make waveform complex and phases difficult to be recognized.

[7] Three seismic phases are used to constrain the velocity structure near the 660-km discontinuity (Figure 2): the wave propagating above the discontinuity (AB branch), the reflection off the discontinuity (BC branch) and the wave traveling below the discontinuity (CD branch). Since the ray paths of these three phases are very close in the shallow proportion of the mantle (Figure 2), the traveltime difference and waveform between these phases are primarily sensitive to the velocity structure near the 660-km discontinuity. The termination distance of the AB branch is sensitive to the velocity gradient above the 660-km discontinuity; the move out of the CD branch is sensitive to the velocity gradient below the 660-km discontinuity; and the traveltime difference between the AB and CD branches is sensitive to the velocity jump across the 660-km discontinuity. The triplication of the 660-km discontinuity occurs in an epicentral distance range of 10° – 35° , so the data in this

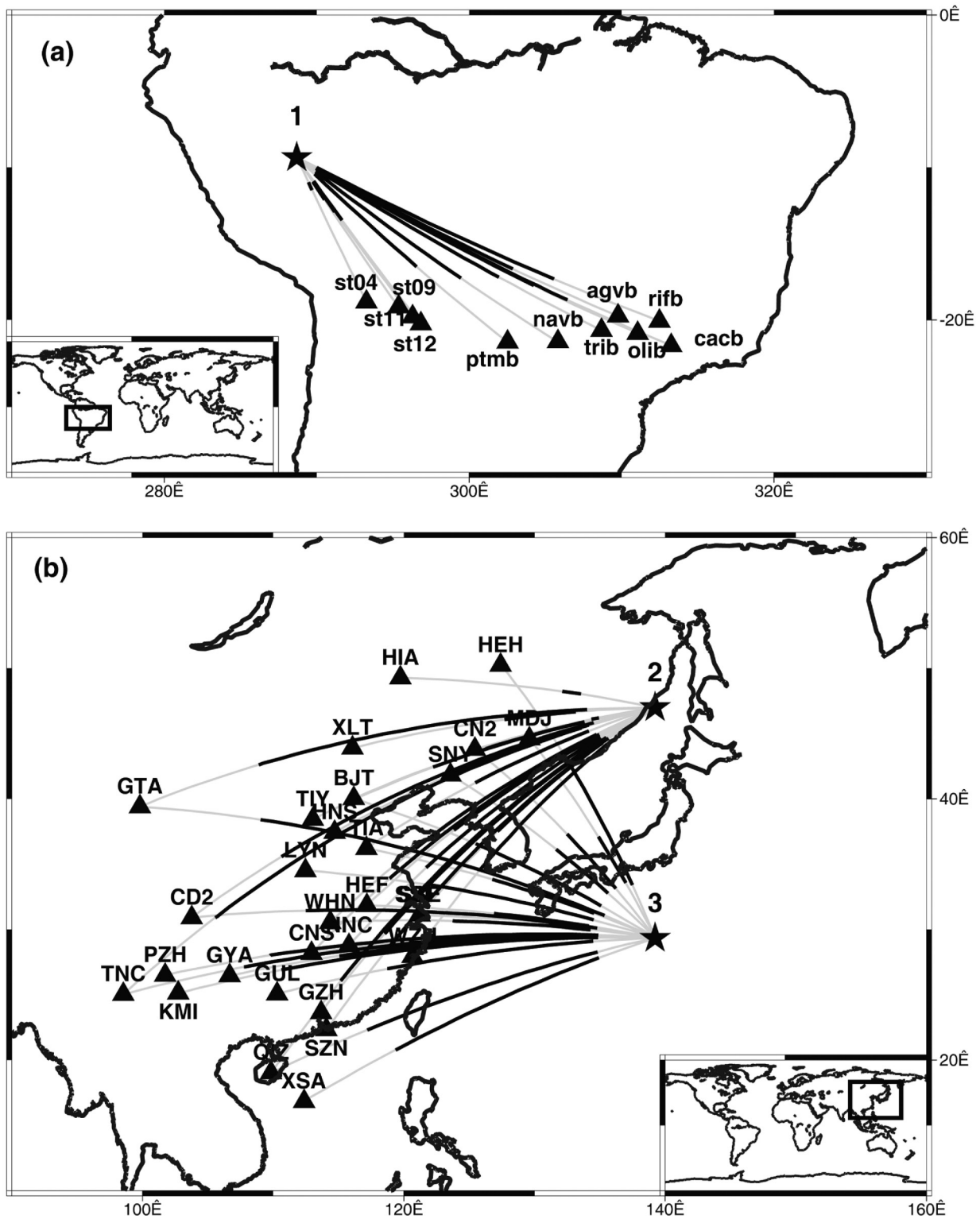


Figure 1. Great circle paths from seismic events (stars) to stations (triangles), with the black segments indicating the portions that the CD branch travels below the 660-km discontinuity, in two study regions: (a) South America (event 1) and (b) northeast Asia (events 2 and 3) (see Table 1 for event information).

Table 1. Event List

Event	Origin Date	Origin Time, UT	Latitude, °N	Longitude, °E	Depth, km
1	4 Nov 1994	0113:20	-9.33	-71.30	597
2	27 Jul 2003	0625:31	47.15	139.25	477
3	2 Aug 2002	2311:39	29.35	139.25	442

epicentral distance range is used. Seismic data are bandpass filtered in a frequency range of 0.04–0.4 Hz.

3. Seismic Shear Velocity Structure Beneath South America

[8] Tangential displacements recorded in the two PASSCAL experiments for event 1 constitute a good record section sampling the seismic structure near the 660-km discontinuity beneath South America (black traces, Figures 3a and 3b). The event exhibits a simple source time function and three branches of triplication are clearly identifiable in the distance range of 10° – 27° . The AB branch turns about 600 km deep in the transition zone at an epicentral distance of 10° and starts to diffract at the top of the 660-km discontinuity at an epicentral distance of about 20° . The CD phase crosses over the AB phase at about 15°

and samples the top of the lower mantle to a depth of 820 km at 27° . The AB branch can be clearly observed in the data after the crossover (see data at stations PTMB, NAVB) until at a distance of about 20° and becomes indiscernible at stations TRIB, AGVB, OLIB, RIFB and CACB at larger distances (Figures 3a and 3b).

[9] PREM [Dziewonski and Anderson, 1981] cannot explain the seismic data sampling South America. The termination distance of the AB branch is larger in the PREM synthetics than in the data, and the traveltime separation between the AB and BC branches is smaller in the synthetics than in the data (Figure 3a).

[10] A larger velocity gradient above the 660-km discontinuity and a deeper 660-km discontinuity are needed to explain the seismic data for event 1. A larger velocity gradient above the discontinuity would make the AB branch terminated at a closer distance as observed in the data; and a deeper discontinuity would predict a larger traveltime difference between the AB and BC branches. We obtain our best fitting model by searching models with various velocity gradients above the discontinuity and various depths of the discontinuity. The best fitting model has a velocity gradient of 0.0024 (km/s)/km above the discontinuity and a deeper 660-km discontinuity at 685 km (Figure 3c). Synthetics calculated using this modified model match well the termi-

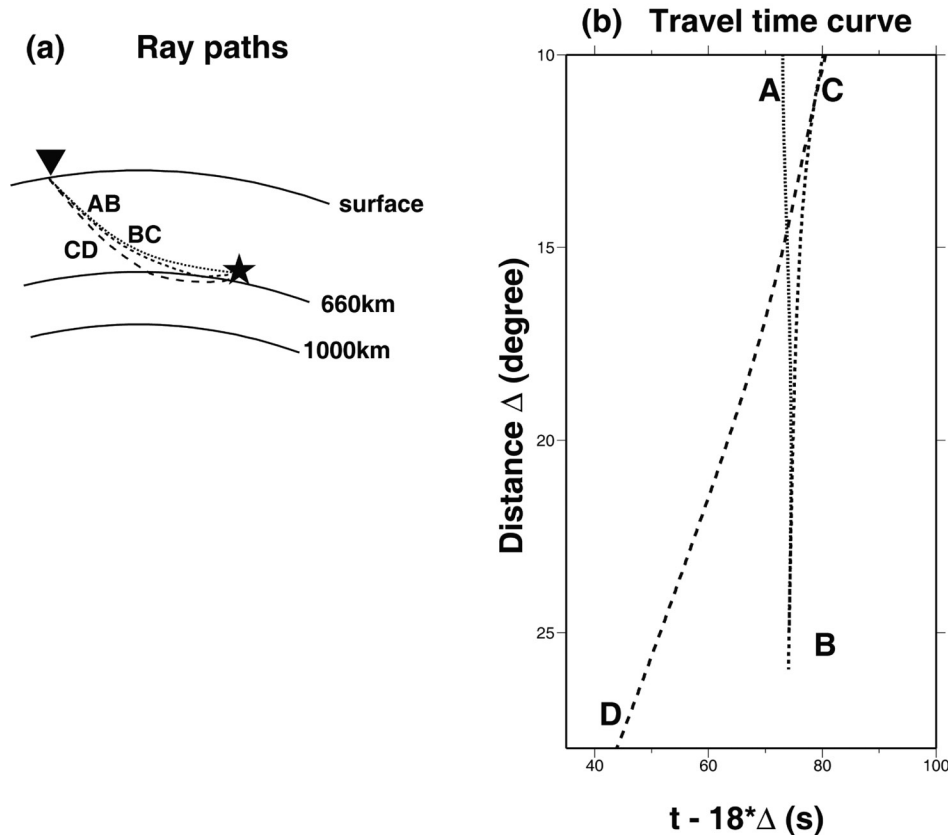


Figure 2. (a) Ray paths and (b) traveltime curves of the triplications near the 660-km discontinuity for a source depth of 597 km. The AB branch is the direct SH wave propagating above the discontinuity; the BC branch is the reflection off the discontinuity; and the CD branch is the seismic wave traveling below the discontinuity.

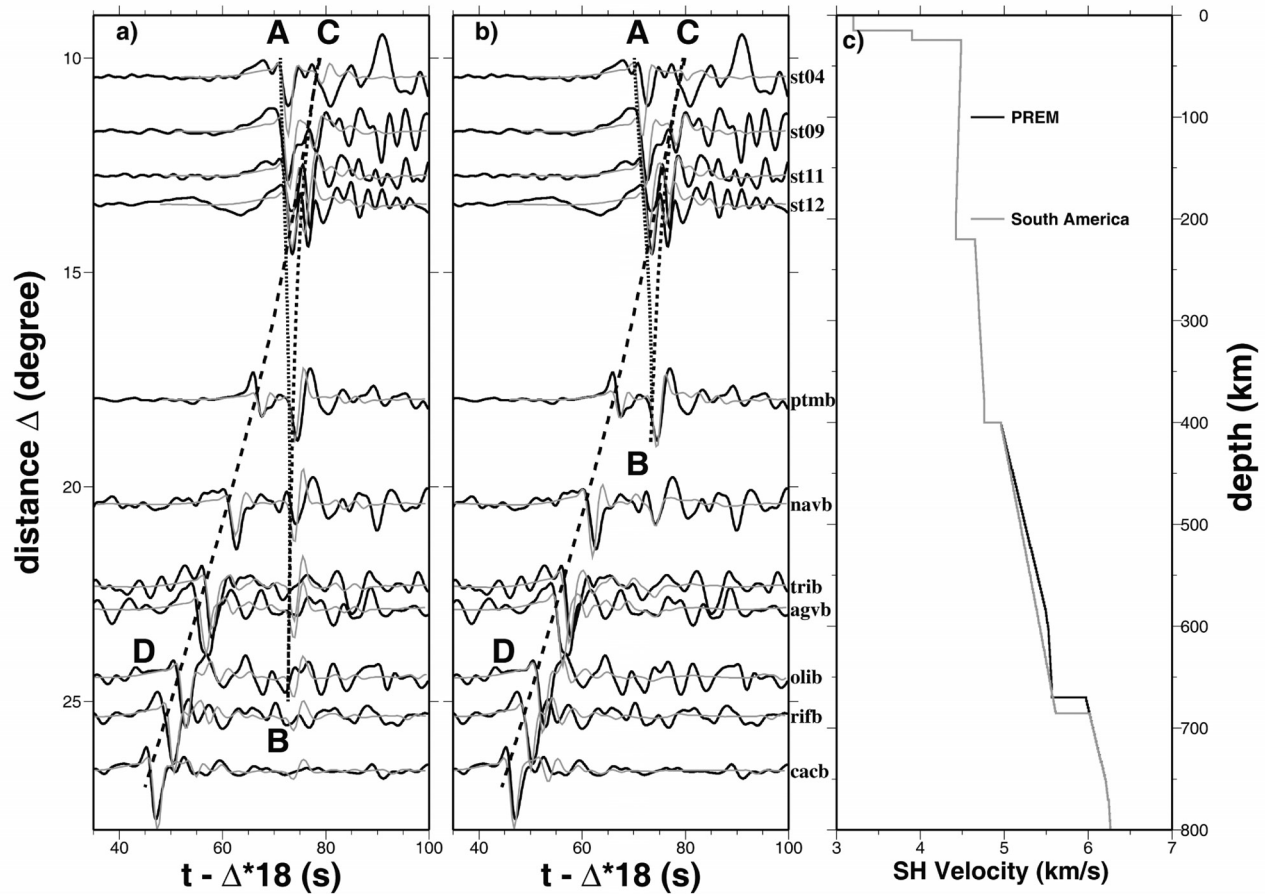


Figure 3. Comparisons of observed tangential displacements for the seismic waves sampling the transition zone beneath South America (event 1) (black traces) and synthetic waveforms (gray traces) calculated using (a) PREM and (b) our best fitting model, along with predicted traveltimes curves of the three branches of the seismic phases (dashed lines). (c) Models. Station traveltimes corrections are made for following stations: TRIB (−1.5 s), OLIB (−1.0 s), RIFB (−0.5 s), based on the observations from another event.

nation distance of the AB branch and the traveltime difference between the AB and BC branches (Figure 3b).

[11] The velocity jump crosses the 660-km discontinuity and the velocity gradient below the discontinuity in PREM, on the other hand, can well explain the data (Figure 3b). The velocity jump across the 660-km discontinuity and the velocity gradient below the discontinuity are well constrained by the crossover distance, and the relative timing and move out of the CD phase observed in the seismic data. For example, synthetic waveforms calculated using a smaller velocity jump across the 660-km discontinuity show a smaller traveltime difference between the AB and CD branches than what observed in the data (Figure 4a). Synthetic waveforms calculated using a smaller velocity gradient below the 660 km discontinuity exhibit a different move out of the CD branch from that in the data (Figure 4b).

[12] The depth of the 660-km discontinuity is, however, not well constrained by the seismic data. It trades off the assumed event depth, and thus strongly depends on the accuracy of the event depth determination. For example, synthetic waveforms calculated using a model with a 15-km shallower 660-km discontinuity and a 15-km shallower

event depth are indistinguishable from those predicted by our preferred model (Figure 4c). The determination of the absolute depth of the 660-km discontinuity would require accurate determination of event depth from other means.

4. Seismic Shear Velocity Structure Beneath Northeast Asia

[13] Tangential displacements recorded in the NCDSN for events 2 and 3 constitute a good record section sampling the seismic structure near the 660-km discontinuity beneath northeast Asia (black traces, Figure 5 for event 2 and Figure 6 for event 3). Three branches of triplication are clearly identifiable in the distance range of 10° – 35° . The AB branch turns about 480 km deep in the transition zone at an epicentral distance of 10° and starts to diffract at the top of the 660-km discontinuity at an epicentral distance of about 30° . For event 2, the AB branch can be clearly observed at stations HNS, TIY, HEF, WZH, WHN, NNC, CNS, GTA, and becomes indiscernible at stations GZH, CD2, SZN at distances greater than 30° (Figure 5). The CD phase crosses over the AB phase at about 19° (Figure 5) and

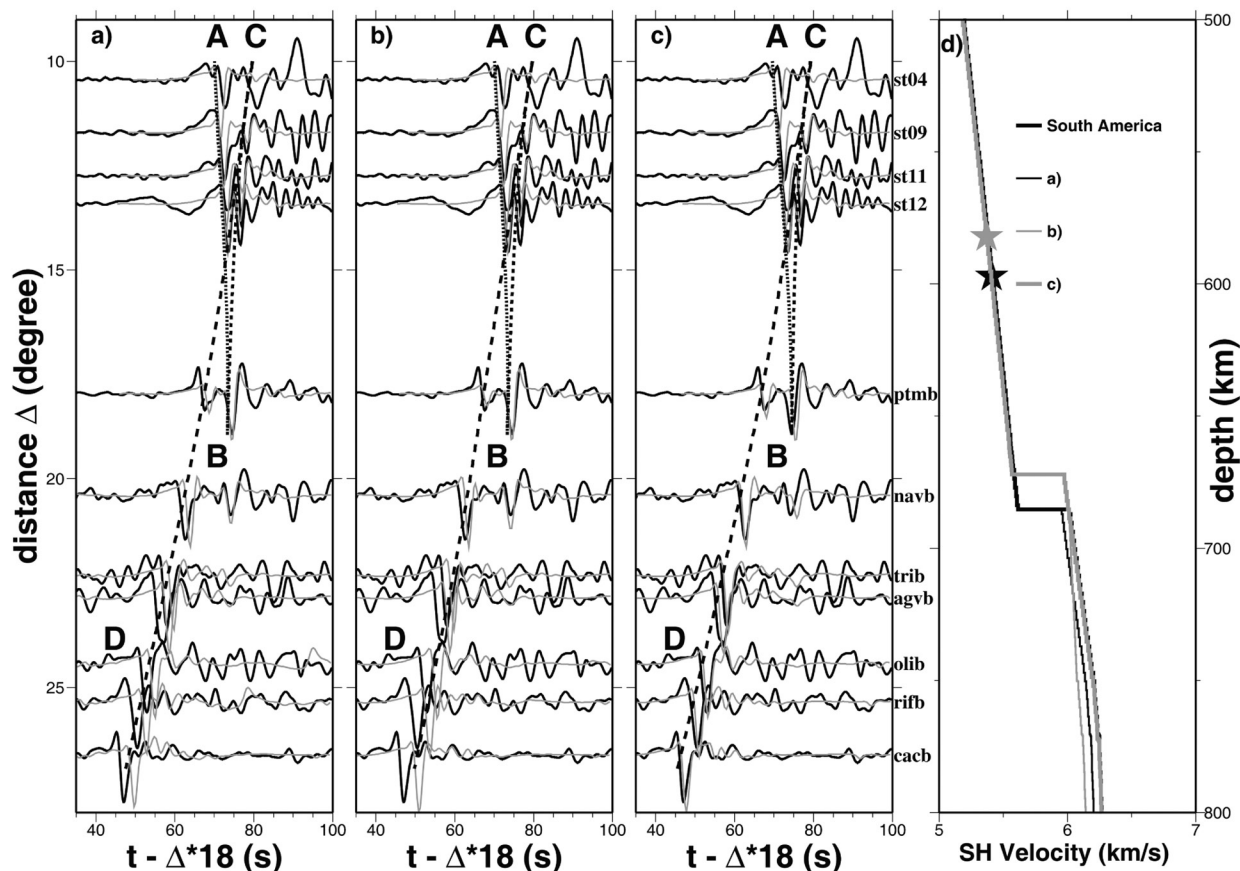


Figure 4. Comparisons of observed tangential displacements for event 1 (black traces) and synthetic waveforms (gray traces) calculated using models perturbed from our best fitting model: (a) with a smaller velocity jump across the discontinuity, (b) with a smaller SH velocity gradient below the discontinuity, and (c) with a 15-km shallower discontinuity, along with predicted traveltime curves of the three branches of the seismic phases (dashed lines). (d) Models, labeled accordingly with the synthetics panels. Synthetics in Figure 4c are calculated with an event depth 15 km shallower. Stars in Figure 4d represent source depths used in the calculations. Same station corrections are made as in Figure 3.

samples the top of the lower mantle to a depth of about 910 km at 35° . For event 3, the AB branch can be clearly observed at stations WHN, BJT, CNS, LYN, GUL, XSA, QIZ, GYA, and becomes indiscernible at stations CD2, KMI, PZH, GTA at distances larger than 30° in the data (Figure 5). The CD phase crosses over the AB phase at about 19.5° (Figure 6) and samples the top of the lower mantle to a depth of about 910 km at 35° .

[14] PREM also cannot explain the seismic data for events 2 (Figure 5a) and 3 (Figure 6a). For both events, the predicted traveltime difference between the AB and CD branches is larger and the crossover of the CD branch occurs at an earlier distance in the PREM synthetics than in the data. A deeper 660-km discontinuity with a larger velocity jump across the discontinuity is needed to explain the observed traveltime features and the crossover distance in the seismic data for both events.

[15] We obtained our best fitting model by searching models with various velocity jumps across the discontinuity and various depths of the discontinuity. The best fitting model has PREM velocity gradients in the transition zone, a velocity jump of 0.53 km/s across the discontinuity, a large

PREM-like velocity gradient extending 80 km below the 660-km discontinuity and a deeper discontinuity at 730 km (Figures 5c and 6c). Synthetics calculated based on our best fitting model fit the observed traveltime differences between the AB and BC branches, crossover distance, and move out of the CD phase, and overall waveforms well (Figures 5b and 6b).

[16] The velocity jump across the discontinuity of our best fitting model is larger than that of PREM and it is well constrained by the traveltime difference between the AB and CD branches in the seismic data for both events. The velocity jump across the discontinuity is tightly constrained by the observed traveltime difference between the AB and CD branches. A larger (smaller) velocity jump would predict a relatively earlier (later) arrival of the CD phase and a larger (smaller) time separation between the two phases. We show an example for a model with a larger velocity jump across the 660-km discontinuity in Figures 7a and 8a. Note that the synthetics show earlier arrivals of the CD phases and larger traveltime differences between the AB and CD branches than in the data (Figures 7a and 8a).

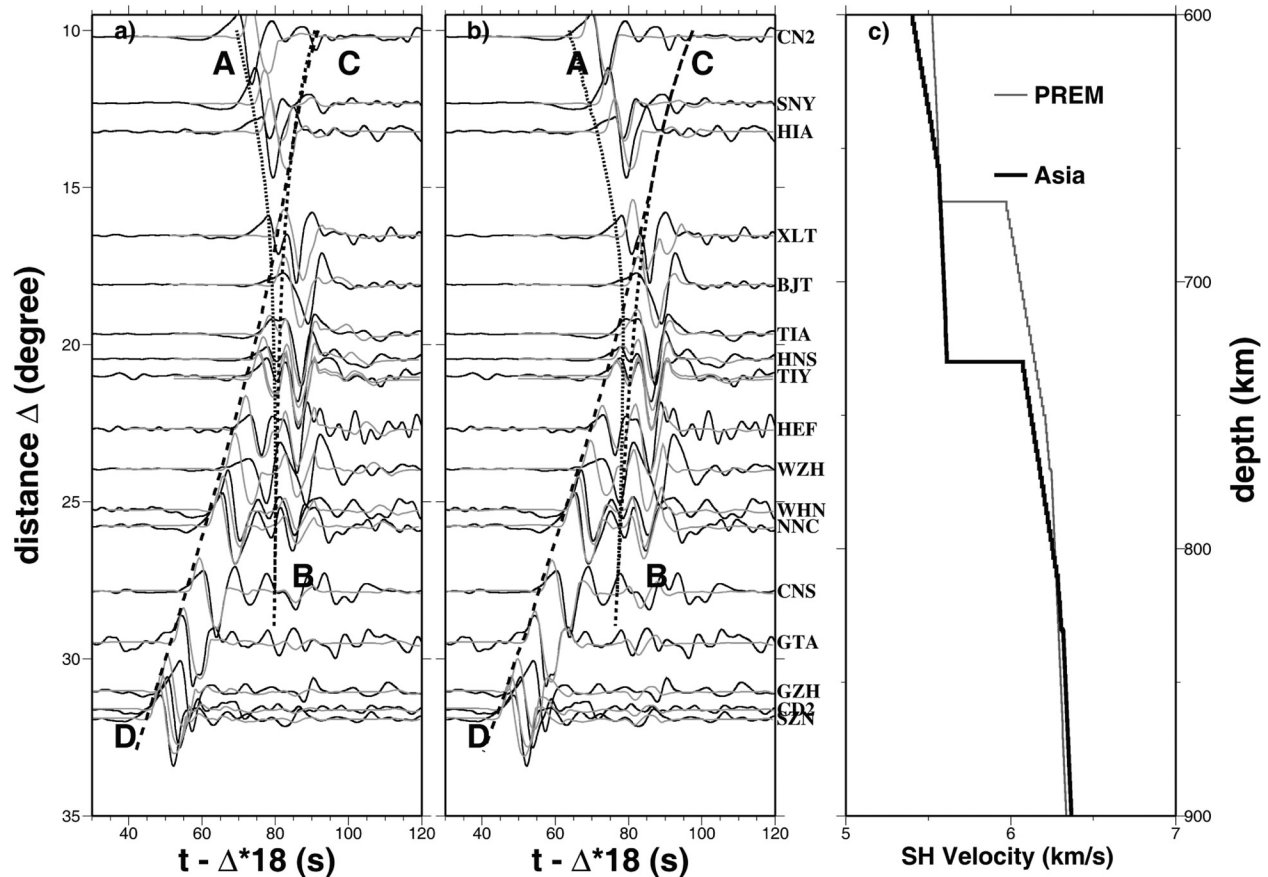


Figure 5. Comparisons of observed tangential displacements for event 2 sampling northeast Asia (Figure 1) (black traces) and synthetic waveforms (gray traces) calculated using (a) PREM and (b) our best fitting Asia model, along with predicted traveltime curves of the three branches of the seismic phases (dashed lines). (c) Models. Station traveltime corrections are made for following stations: CN2 (2 s), SNY (2 s), TIA (2 s), HNS (2 s), TIY (2 s), GTA (2.5 s), based on the observations from another event.

[17] The PREM-like velocity gradient below the 660-km discontinuity in our best fitting model is also well resolved by the seismic data. The observed move out of the CD phase is sensitive to the velocity gradient below the discontinuity. For example, synthetics calculated based on a model with a larger velocity gradient below the 660-km discontinuity show a different move out of the CD branch from that in the data (Figures 7b and 8b).

[18] The depth extent of the large velocity gradient below the 660-km discontinuity is also well constrained by the seismic data. A shallower depth extent of the large velocity gradient below the 660-km discontinuity predicts later CD phases in the synthetics at large distances than in the data (Figures 9a and 10a), while a deeper depth extent predict earlier CD phases in the synthetics at large distances (Figures 9b and 10b).

[19] The best fitting PREM-like velocity gradient just above the 660-km discontinuity is well constrained by the termination distance of the AB branch in the seismic data. The larger the velocity gradient above the discontinuity, the smaller the termination distance of the AB branch. We show an example of comparison of the data and synthetics for a model with a larger velocity gradient just above the discon-

tinuity (Figures 11a and 12a). Note that, for a larger velocity gradient above the discontinuity, the synthetics show an indiscernible AB phase at large distances ($>27^\circ$) and a weak AB phase at about 26° , while the data exhibit a strong AB phase up to 33° (Figures 11a and 12a).

[20] The seismic data sampling northeast Asia also require a change of velocity gradient about 70 km above the 660-km discontinuity, same as PREM. PREM has two velocity gradients in the transition zone, with one (0.0029 (km/s)/km) between 400 km and 600 km depths and the other (0.0007 (km/s)/km) between 600 km and 670 km. Note that, while a smaller velocity gradient would explain the termination distance of the AB branch in the seismic data, it would also predict a strong phase traveling in shallow portion of the transition zone (pointed by arrows in Figures 11b and 12b). No such phase is visible in the data. When the velocity gradient in the lowermost transition zone is fixed, changing the velocity gradient in the upper transition zone does not affect the termination distance of the AB branch. It would, however, generate different amplitudes and traveltimes for the phase traveling in the upper transition zone. A larger velocity gradient would predict a weak phase traveling in the shallow part of the

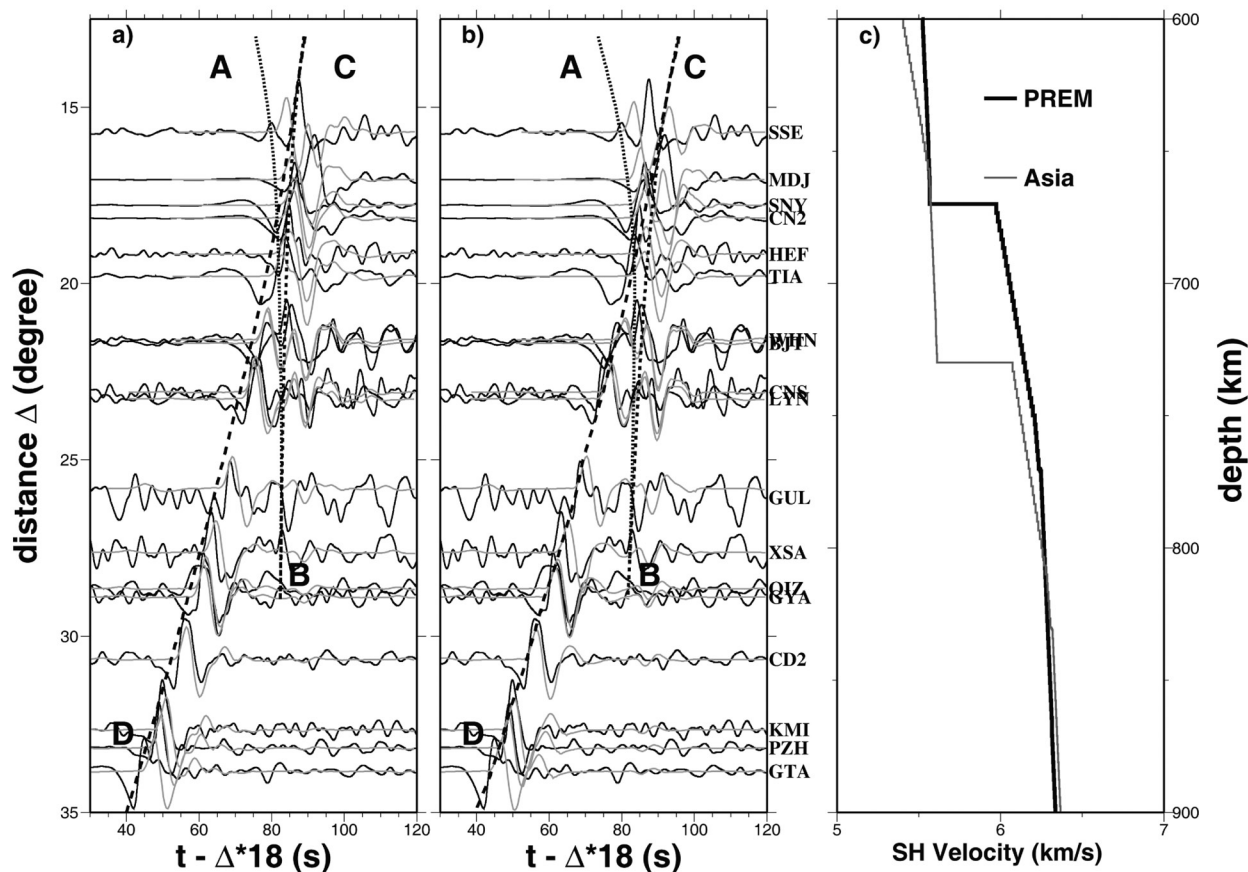


Figure 6. Comparisons of observed tangential displacements for event 3 sampling northeast Asia (Figure 1) (black traces) and synthetic waveforms (gray traces) calculated using (a) PREM and (b) our best fitting Asia model, along with predicted traveltime curves of the three branches of the seismic phases (dashed lines). (c) Models. Station traveltimes corrections are made for following stations: CN2 (2 s), SNY (2 s), GYA (−1.5 s), KMI (3 s), PZH (0.5 s), based on the observations from another event.

transition zone, but it would make the AB branch terminated at closer distances than in the data. In another word, the termination distance of the AB branch observed in the data requires a small velocity gradient in the lower part of the transition zone, whereas the fact the phase traveling in the upper part of the transition zone is invisible in the data requires a large velocity gradient in the upper part of the transition zone. The seismic data thus indicate different velocity gradients in the lower (lowermost 70 km) and upper parts of the transition zone.

[21] The seismic data for events 2 and 3, although sample the transition zone beneath Northeast Asia in the directions perpendicular to each other, can be explained by a same SH velocity model (e.g., Figures 5b and 6b). The consistency of the results obtained from the two events indicates that the effect of lateral variation of seismic velocity is not significant in our sampling region and the one-dimensional waveform modeling is appropriate.

5. Compositional and Mineralogical Models Beneath South America and Northeast Asia

[22] In this section, we infer mantle mineralogical models in the two regions through quantitative comparisons be-

tween the seismic models obtained from modeling the seismic data and the velocity structures predicted based on various mineralogical models. We also explore the conditions of mantle composition and temperature that are appropriate for explaining the difference of the inferred mineralogical models between the two regions.

[23] Mantle composition consists of two major components: an olivine-normative ($(Mg, Fe)_2SiO_4$) component and a pyroxene-normative ($(Mg, Fe)SiO_3$) component. At a pressure of approximate 14 GPa, corresponding to the depth of the 410-km discontinuity, olivine (α phase) transforms to wadsleyite (β phase) and pyroxene transforms to garnet, with increases in seismic velocity and density. At a depth of about 520 km, wadsleyite transforms to ringwoodite (γ phase). Near the 660-km discontinuity, garnet transforms to perovskite and ringwoodite transforms to perovskite plus magnesio-wustite. The transformation from ringwoodite to perovskite plus magnesio-wustite completes in a depth range of less than 2 km. At low mantle temperature or/and low Al content (Table 2), garnet could transform to ilmenite first in the bottom of the transition zone before it starts to transform to perovskite across the 660-km discontinuity. Depending on mantle composition (mostly Al content), the garnet trans-

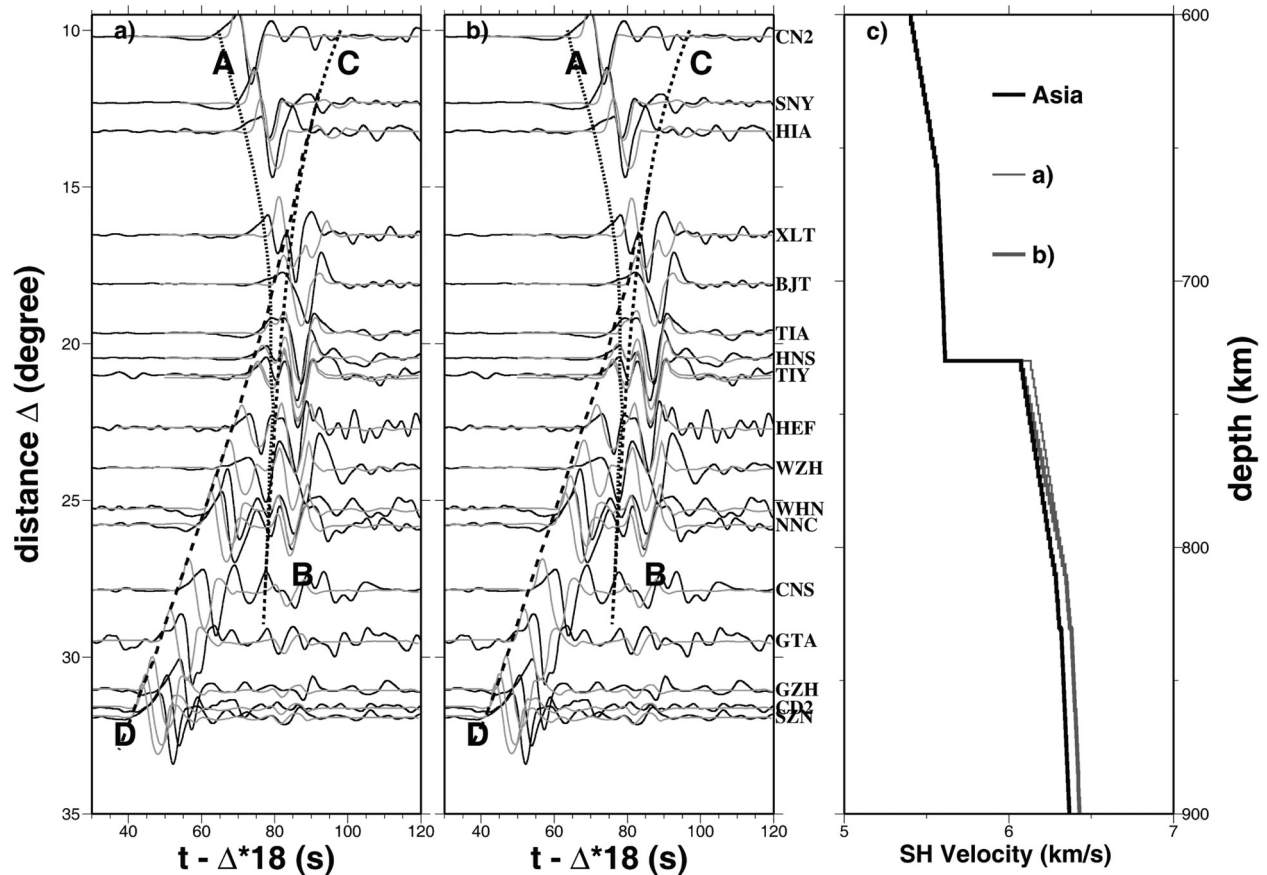


Figure 7. Comparisons of tangential displacements observed for event 2 (black traces) and synthetic waveforms (gray traces) calculated using two models perturbed from the best fitting Asia model: (a) with a larger velocity jump across the 660-km discontinuity and (b) with a larger velocity gradient below the discontinuity, along with predicted traveltime curves of the three branches of the seismic phases (dashed lines). (c) Models, labeled accordingly with the synthetics panels. Station corrections are made as in Figure 5.

formation to perovskite could persist to 100 km below the 660-km discontinuity.

[24] The velocity gradient above the 660-km discontinuity is controlled by temperature and pressure dependencies of the elastic properties of major mineral phases (ringwoodite + garnet + Ca-perovskite) and, if ilmenite is present, the increasing volume fraction of ilmenite with depth. The velocity jump across the 660-km discontinuity is sensitive to the volume fraction of ringwoodite in the composition and the fraction of garnet transformed to perovskite across the discontinuity. The velocity gradient below the discontinuity is determined by temperature and pressure dependencies of the elastic properties of major mineral phases (perovskite + magnesiowustite + Ca-perovskite + garnet) and the decreasing volume fraction of garnet (or increasing volume fraction of perovskite) with depth. The decreasing volume fraction of garnet would generate a large velocity gradient in the top of the lower mantle. The depth extent of the high-velocity gradient below the 660-km discontinuity is sensitive to the volume fraction of garnet present after its first-order transformation at the 660-km discontinuity, which is sensitive to the aluminum content of mantle composition (Table 3), but less so to mantle temperature.

[25] In mineral physics modeling, seismic velocities near the 660-km discontinuity are calculated following the procedures outlined by *Weidner and Wang* [1998]. We use phase equilibria data to define the stable assemblages at relevant pressures and temperatures and cation distribution data to define the chemical composition of each phase. This information, along with our current estimates of physical properties of these phases [*Weidner and Wang*, 1998, Table 1], provides a mineralogical model with volume fractions of each phase along with the aggregate velocities and density. In this calculation, we use the phase diagram of CaO-MgO- Al_2O_3 - SiO_2 (CMAS) system reported by *Gasparik* [1996] as a template for defining the evolution of the system through perovskite formation processes. Clapeyron slopes of $-2 \text{ MPa}^\circ\text{C}$ and $+2.5 \text{ MPa}^\circ\text{C}$ are used for the ringwoodite to perovskite plus magnesiowustite transition and the garnet-to-perovskite transition, respectively. Al contents in ringwoodite and ilmenite are assumed to be negligible in these systems [*Gasparik*, 1990] and the Fe/Mg ratio is assumed to be the same for all phases in the calculations.

[26] For PREM, the velocity gradient above the 660 km discontinuity can be explained by the temperature and

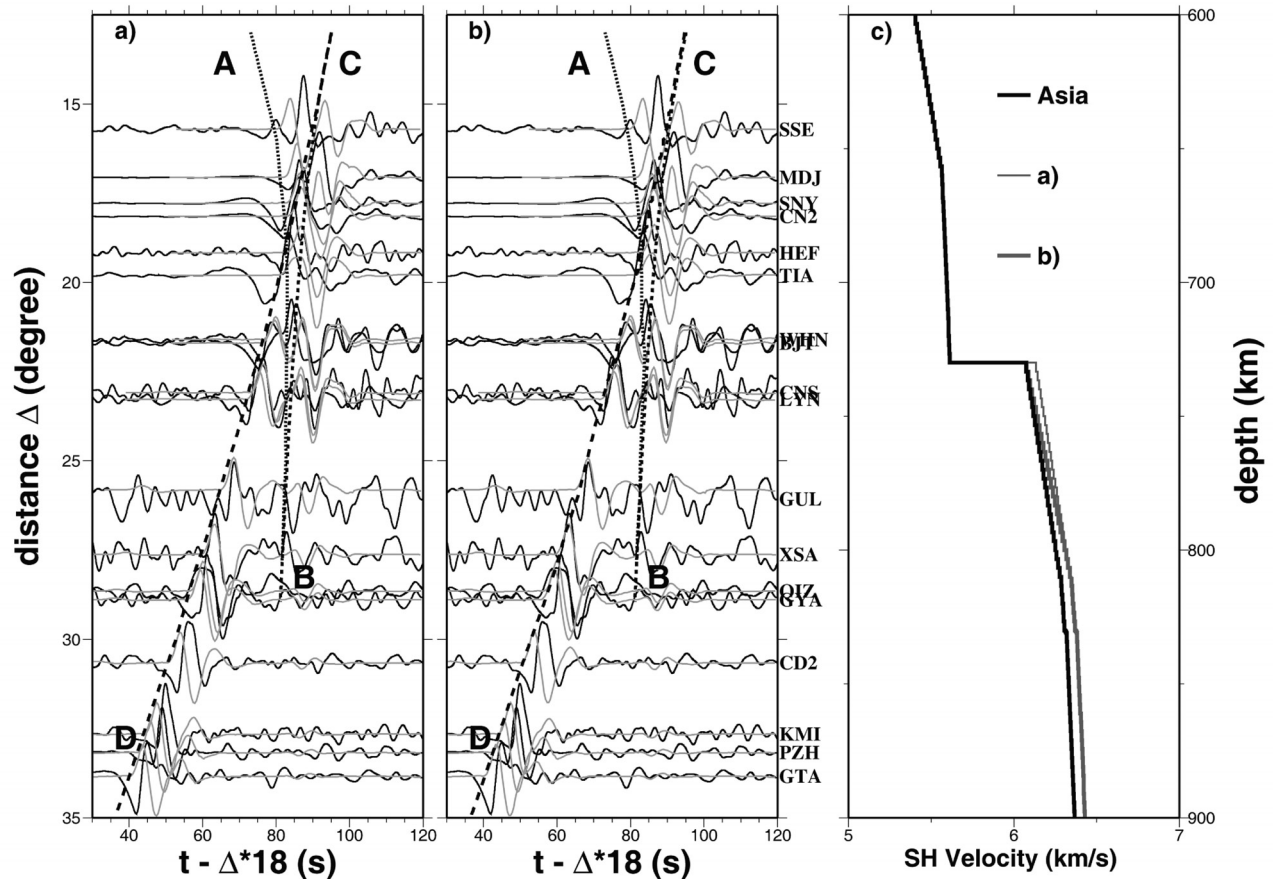


Figure 8. Comparisons of tangential displacements observed for event 3 (black traces) and synthetic waveforms (gray traces) calculated using two models perturbed from the best fitting Asia model: (a) with a larger velocity jump across the 660-km discontinuity and (b) with a larger velocity gradient below the discontinuity, along with predicted traveltime curves of the three branches of the seismic phases (dashed lines). (c) Models, labeled accordingly with the synthetics panels. Station corrections are made as in Figure 6.

pressure dependencies of the elastic properties of the major phases (ringwoodite + garnet + Ca-perovskite) (Figure 13a). The velocity jump can be explained by the pyrolite model (37.8% garnet and 54% ringwoodite). The velocity gradient below the 660-km discontinuity of PREM can be explained by the temperature and pressure dependencies of the elastic properties of major mineral phases (perovskite + magnesio-wustite + Ca-perovskite + garnet) and the decreasing volume fraction of garnet with depth in a mantle composition with an aluminum content of 3.4%.

[27] Beneath South America, the temperature and pressure dependencies of the elastic properties of the major phases cannot explain the large velocity gradient above the 660-km discontinuity, and existence of ilmenite is needed to explain the gradient (Figure 13b). Because the shear wave velocity of ilmenite is larger than that of garnet, increasing volume fraction of ilmenite results in a large velocity gradient above the 660-km discontinuity. In order to maintain the velocity jump across the discontinuity and the depth extents of the high-velocity gradient below this discontinuity to be similar to PREM, in the presence of the ilmenite phase in the bottom of the transition zone, a larger volume fraction of garnet in bulk composition model is needed

beneath South America. The depth extent of the high-velocity gradient below the 660-km discontinuity (about 80 km, Figure 13b) indicates a mantle composition with an aluminum content of 3.4% in the top of the lower mantle.

[28] Beneath northeast Asia, the velocity gradient above the 660-km discontinuity can be explained by the temperature and pressure dependencies of elastic properties of the major phases in the transition zone (ringwoodite + garnet + Ca-perovskite) (Figure 13c). The large velocity jump across the discontinuity requires a larger fraction of garnet transforming to perovskite across the discontinuity than what is required for explaining PREM. The inferred depth extent of the high-velocity gradient below the 660-km discontinuity (about 80 km) would indicate a mantle composition with an aluminum content of 3.4% in the top of the lower mantle in this region.

[29] Our mineral physics modeling indicates that our seismic results can be explained by a uniform composition with aluminum content of 3.4% in the lower mantle between the two regions. If we assume that the mantle have a uniform composition in these two regions, our inferred seismic structures would indicate different temperatures in the transition zone between the two regions. For a mantle

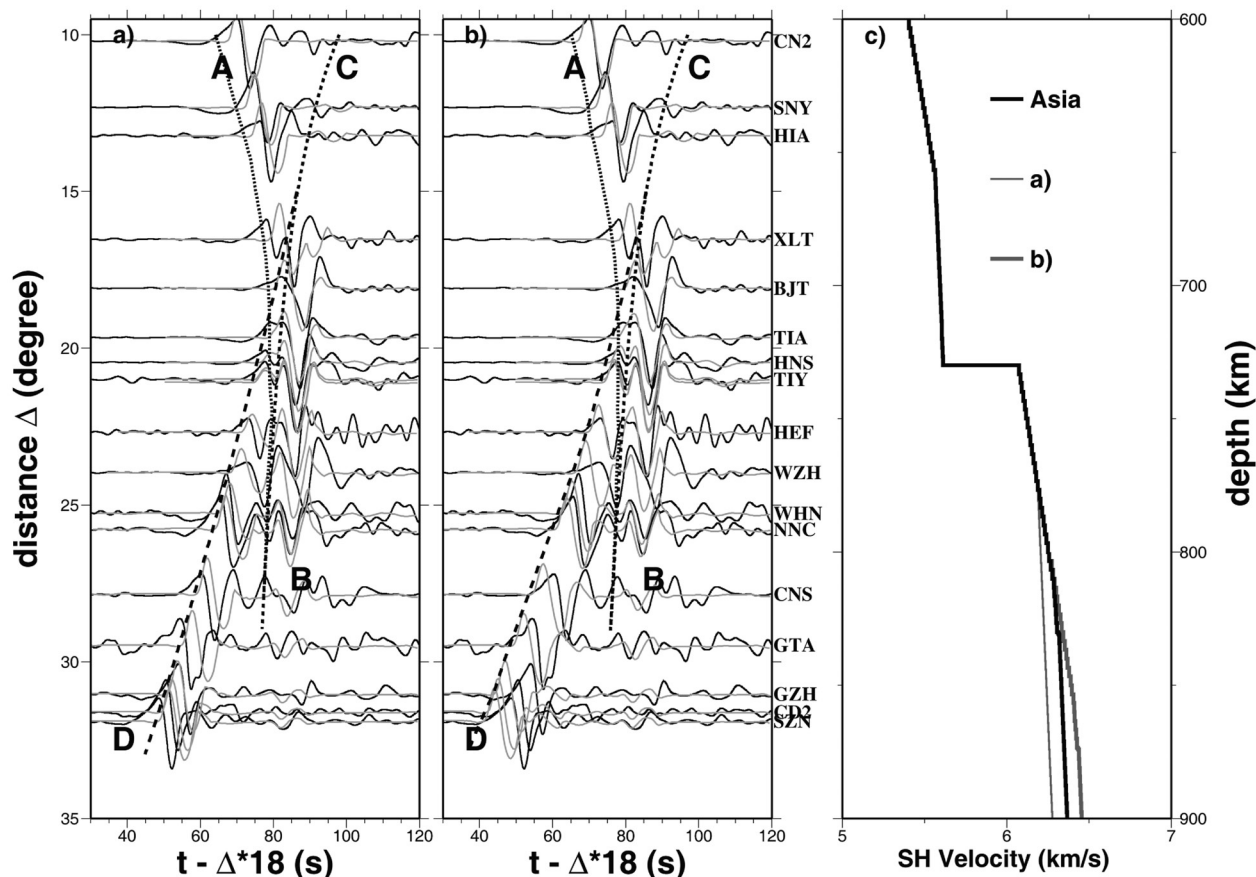


Figure 9. Comparisons of tangential displacements observed for event 2 (black traces) and synthetic waveforms (gray traces) calculated using two models perturbed from the best fitting Asia model: (a) with a smaller depth extent of the larger velocity gradient below the 660-km discontinuity and (b) with a larger depth extent of the larger velocity gradient below the 660-km discontinuity, along with predicted traveltime curves of the three branches of the seismic phases (dashed lines). (c) Models, labeled accordingly with the synthetics panels. Station corrections are made as in Figure 5.

composition with an aluminum content of 3.4%, the existence of ilmenite beneath South America would suggest a mantle temperature (at 660 km) lower than 1334°C and the absence of ilmenite beneath northeast Asia would require a mantle temperature higher than 1434°C. That means a mantle temperature difference of at least 100°C between two regions. The inferred absolute mantle temperatures are subject to the uncertainties in the experimental measurements of the elastic properties, but the temperature difference is not.

[30] As the other end-member of the explanations, the seismic structures above the 660-km discontinuity between the two regions can also be explained by different mantle compositions with different aluminum contents without invoking a temperature difference between the two regions. In this case, the aluminum content of the mantle composition should be lower beneath South America because of the presence of ilmenite there. If, for example, we assume mantle temperature (at 660 km) in these two regions is 1334°C, the aluminum content in mantle composition is about 3.4% beneath South America to explain the presence of ilmenite there and should be higher than 4.6% beneath

northeast Asia to explain the absence of ilmenite there. An aluminum content difference of more than 1% is required between the two regions. The inferred absolute aluminum content depends on the assumed mantle temperature, but the inferred difference in aluminum content between the two regions does not.

6. Double 660-km Discontinuities

[31] In sections 2–5, we have assumed a single discontinuity at the bottom of the transition zone in both the seismic and mineral physics modeling. Since two phase transformations occur near 660 km and they can occur at different pressures, multiple discontinuities may exist near the 660-km depth. The depths of the phase transformations are controlled by mantle temperature, composition and chemical interaction between the olivine and pyroxene components. The phase transformation from ringwoodite to perovskite plus magnesiowustite is endothermic with a negative Clapeyron slope, while that from garnet to perovskite is exothermic with a positive Clapeyron slope. When mantle temperature is high, the phase transformation from

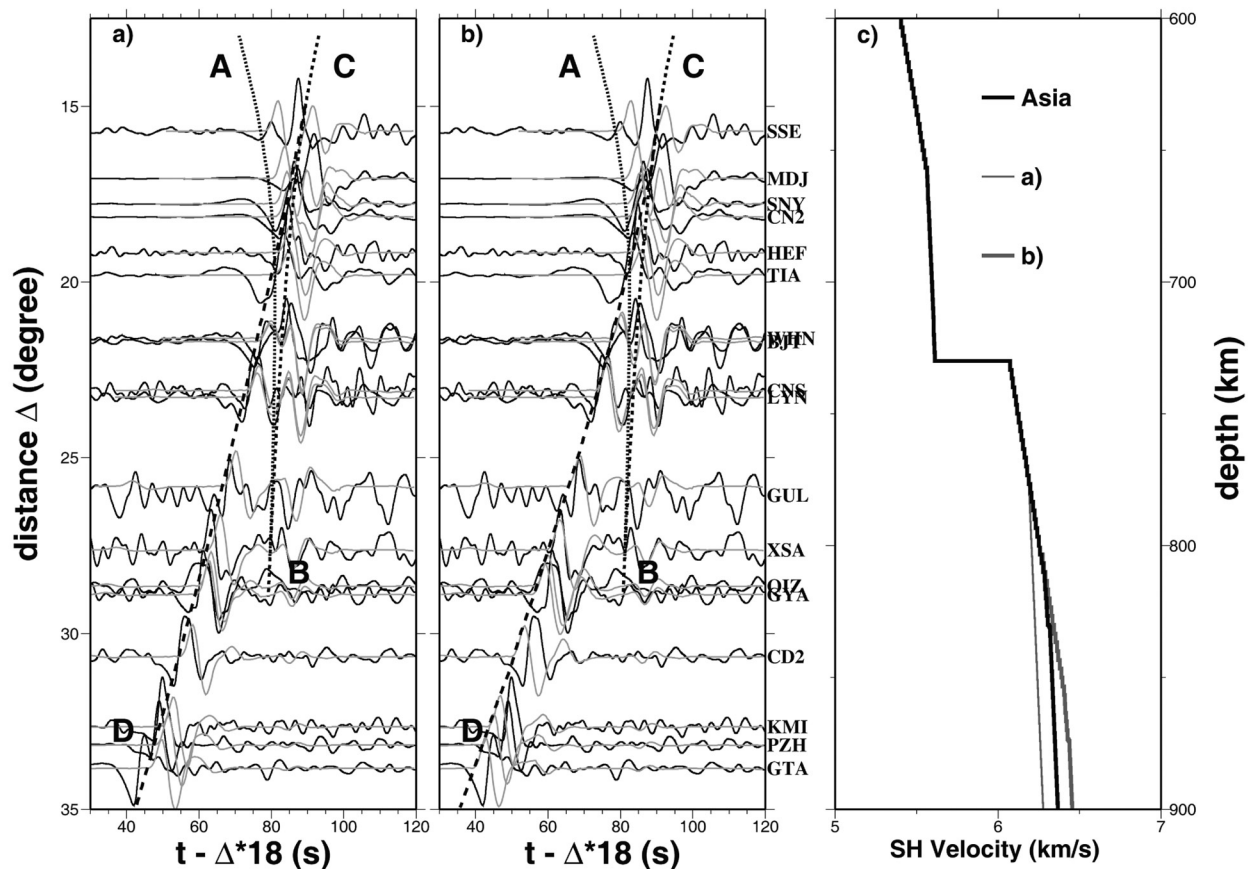


Figure 10. Comparisons of tangential displacements observed for event 3 (black traces) and synthetic waveforms (gray traces) calculated using two models perturbed from the best fitting Asia model: (a) with a smaller depth extent of the larger velocity gradient below the 660-km discontinuity and (b) with a larger depth extent of the larger velocity gradient below the 660-km discontinuity, along with predicted traveltime curves of the three branches of the seismic phases (dashed lines). (c) Models, labeled accordingly with the synthetics panels. Station corrections are made as in Figure 6.

ringwoodite to perovskite plus magnesiowustite occurs at a lower pressure and the phase transformation from garnet to perovskite occurs at a higher pressure, and vice versa. So if these transformations do not interact chemically, they will most likely occur at different pressures and double discontinuities would appear near the 660-km depth. The phase transformation from garnet to perovskite, however, is also sensitive to the Al content in the system. A high Al content would stabilize the garnet phase to higher pressures, and make the garnet phase transformation to perovskite to appear at larger depths. The Al partitions are different between different mineral assemblages. Al would preferentially be partitioned into garnet when garnet, ringwoodite and ilmenite are in coexistent, and would preferentially be partitioned into perovskite in the assemblage of ringwoodite and perovskite. When the phase transformation from ringwoodite to perovskite plus magnesiowustite occurs and at a pressure lower than the phase transformation from garnet to perovskite, some Al would be partitioned into perovskite from garnet. A reduced Al content in garnet would make the phase unstable, and the phase transformation from garnet to perovskite would occur instantaneously at the same pressure (Figure 14a). In this case, a single discontinuity would

appear near the 660-km depth. If, for the mantle temperature and composition that the phase transformation from garnet (and ilmenite, if present) to perovskite occurs at a pressure lower than the ringwoodite transformation to perovskite plus magnesiowustite, double discontinuities would appear near the 660-km depth, with the shallower one resulted from garnet (and ilmenite, if present) to perovskite and the deeper one from the transformation from ringwoodite to perovskite plus magnesiowustite and, in a system with a high Al content, a further transformation from garnet to perovskite (Figures 14b and 14c). Such scenarios could occur when the mantle temperatures are relatively low or/and the Al contents of the system are low. At a high Al content and in the absence of ilmenite, the shallower discontinuity is controlled by the first-order transformation from garnet to perovskite. The deeper discontinuity is controlled by the phase transformation from ringwoodite to perovskite plus magnesiowustite and a further transformation from garnet to perovskite in response to the reduced Al content in garnet because of the increased volume of perovskite after the ringwoodite transformation (Figure 14b). When ilmenite is present, Al would preferentially be partitioned into garnet and the presence of the ilmenite phase would increase the Al

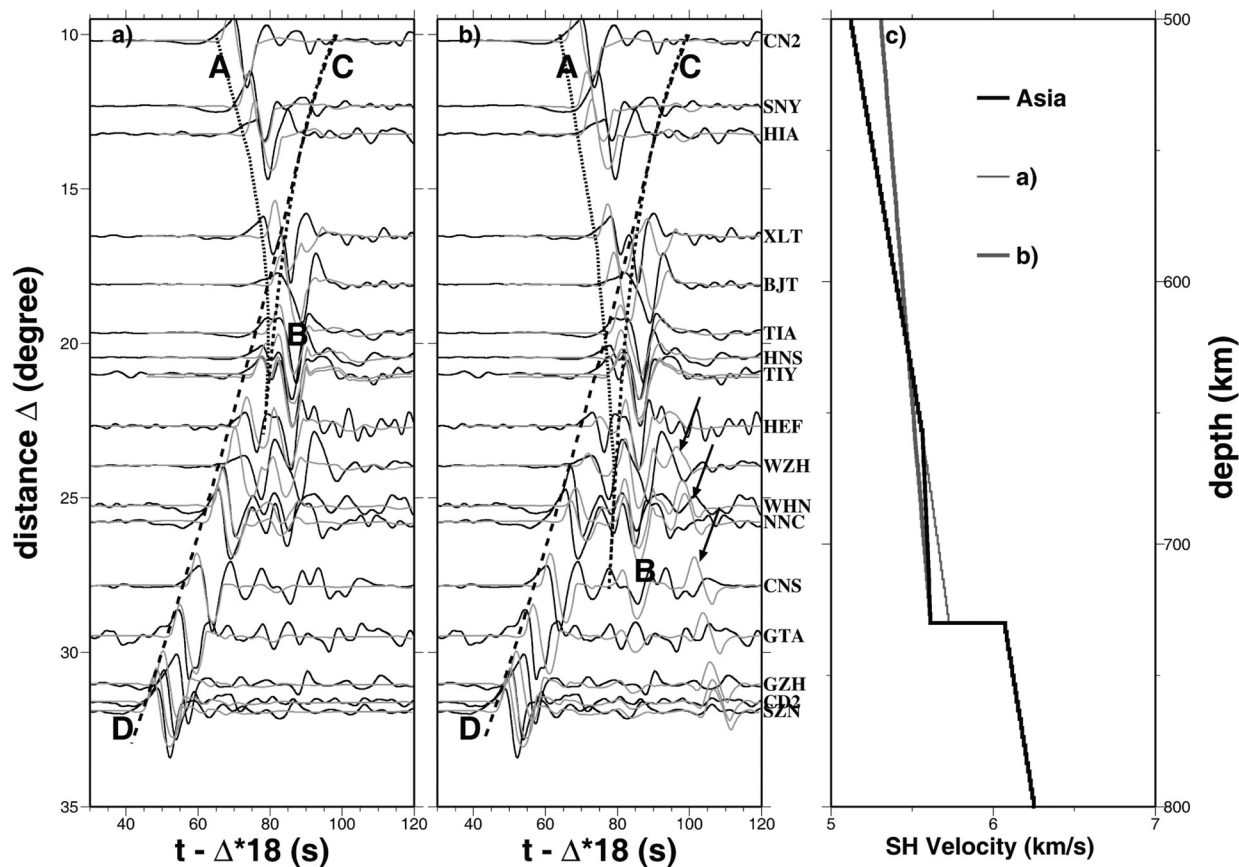


Figure 11. Comparisons of tangential displacements observed for event 2 (black traces) and synthetic waveforms (gray traces) calculated using two models perturbed from the best fitting Asia model: (a) with a different velocity gradient in the bottom 70 km of the transition zone and (b) with a uniform velocity gradient in the transition zone, along with predicted traveltime curves of the three branches of the seismic phases (dashed lines). (c) Models, labeled accordingly with the synthetics panels. Station corrections are made as in Figure 5.

content in garnet and stabilize the garnet phase. However, when ilmenite transforms to perovskite, some Al would be partitioned into perovskite from garnet and a reduced Al content in garnet would make garnet unstable and to transform to perovskite. In this scenario, the shallower discontinuity is controlled by simultaneous transformations of garnet and ilmenite to perovskite and the deeper discontinuity by the phase transformation from ringwoodite to perovskite plus magnesiowustite (Figure 14c).

[32] The depth separation of the double discontinuities is sensitive to mantle temperature and the Al content of the system. A lower mantle temperature would make the phase transformation from ringwoodite to perovskite plus magnesiowustite to occur at a higher pressure and the phase transformation from garnet to perovskite at a lower pressure, so the separation of the discontinuities increases with decreasing temperature. A lower Al content would not change the pressure of the ringwoodite phase transformation, but it would make the phase transformation from garnet to perovskite to occur at a lower pressure, so the separation of the discontinuities increases with decreasing Al content. However, when the Al content and/or mantle

temperature are lowered to some extents, the ilmenite phase starts to appear (such as in the scenario in Figure 14c). The separation of the double discontinuities is then controlled by the pressure difference of the phase transformations from ilmenite to perovskite and from ringwoodite to perovskite plus magnesiowustite, and reaches maximum. The maximum separation of the double discontinuities also becomes insensitive to the Al content and mantle temperature, because these two phase transformation pressures are not sensitive to the Al content, and both phase transformations are endothermic with similar Clapeyron slopes making the pressure difference of these two phase transformations insensitive to temperature.

[33] The velocity jumps of the double discontinuities are different in the two scenarios shown in Figures 14b and 14c. The S velocity jump caused by phase transformation from garnet to perovskite is large (about 8–9%), while that caused by the phase transformation from ringwoodite to perovskite plus magnesiowustite is only about 1%. In the absence of the ilmenite phase (Figure 14b), the velocity jump across the shallower discontinuity is about 2.8% and that across the deeper one is about 3.5%. In the presence of

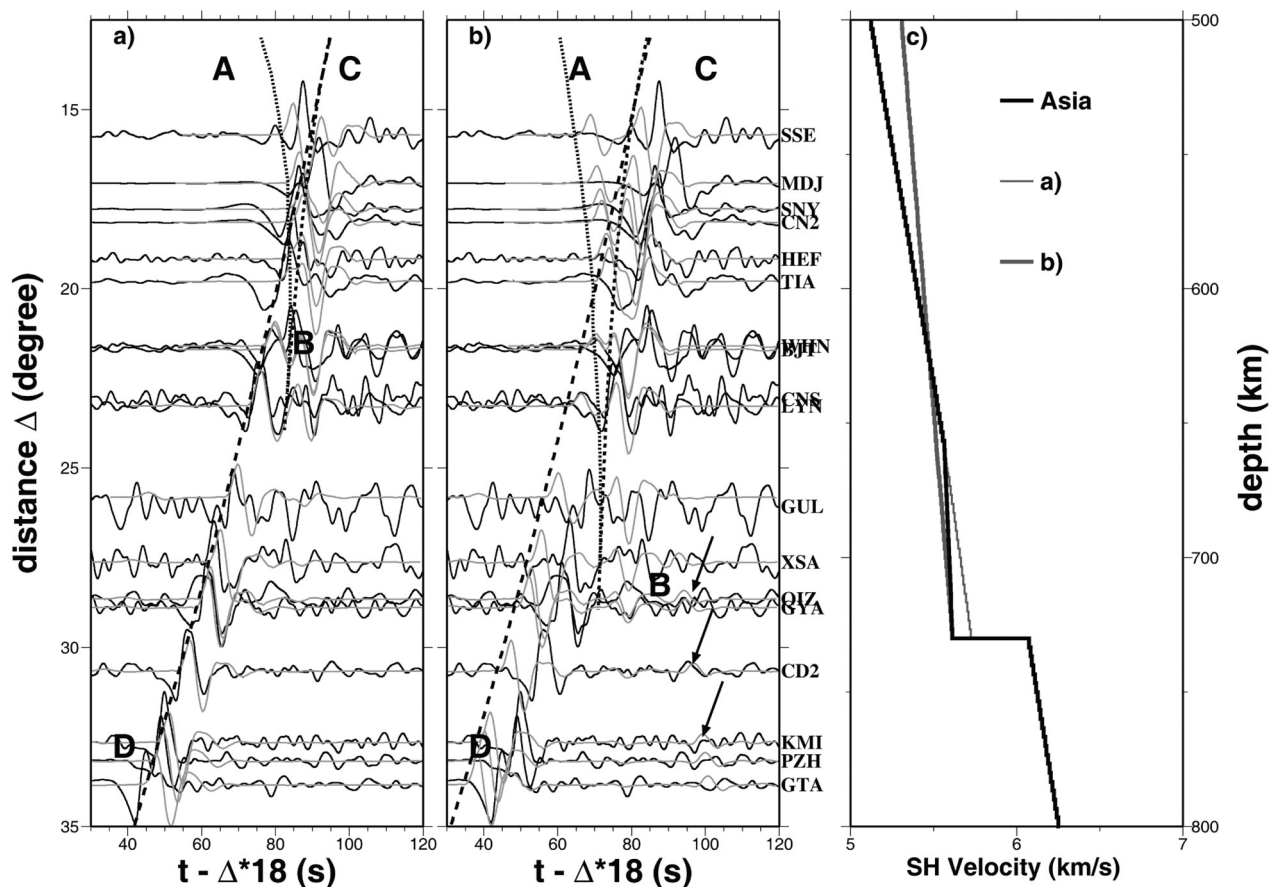


Figure 12. Comparisons of tangential displacements observed for event 3 (black traces) and synthetic waveforms (gray traces) calculated using two models perturbed from the best fitting Asia model: (a) with a different velocity gradient in the bottom 70 km of the transition zone and (b) with a uniform velocity gradient in the transition zone, along with predicted traveltime curves of the three branches of the seismic phases (dashed lines). (c) Models, labeled accordingly with the synthetics panels. Station corrections are made as in Figure 6.

ilmenite (Figure 14c), the velocity jump across the shallower discontinuity is dominant (about 5%) and that of the deep one is about 1%.

[34] Under the inferred mantle temperatures and compositions beneath South America and northeast Asia, the separation between the double discontinuities should be less than 20 km. Beneath South America, with the ilmenite phase present, double discontinuities may exist, similar to the scenario in Figure 14c. The separation between the two discontinuities is controlled by the pressure difference of the phase transformations from ilmenite to perovskite and from ringwoodite to perovskite plus magnesiowustite, and is less than 20 km. Beneath northeast Asia, there is no evidence for the presence of the ilmenite phase. There are two possibilities: (1) the mantle temperature is high, so that the ringwoodite to perovskite plus magnesiowustite phase transformation occurs at a lower pressure and the phase transformation from garnet to perovskite occurs at the same depth, similar to the scenario in Figure 14a; or (2) the Al content is high, double discontinuities exist, with the shallower one caused by the garnet to perovskite phase transformation, and the deeper one by the ringwoodite

transformation to perovskite plus magnesiowustite and a further transformation from garnet to perovskite similar to the scenario in Figure 14b. The separation between the two discontinuities in this case is also within 20 km.

[35] The SH data we used cannot distinguish double discontinuities separated by less than 20 km from a single discontinuity. The synthetics based on a model with two discontinuities separated by 20 km fit the seismic data equally well (Figure 15a). Our seismic data, however, would exclude models with double discontinuities separated

Table 2. Presence of Ilmenite Above the 660-km Discontinuity Versus Aluminum Content and Mantle Temperature

Aluminum Content, %	Temperature of the Presence of Ilmenite, °C
0	any temperature
1	<1694
2	<1534
3	<1434
4	<1347
5	<1334

Table 3. Garnet Below the 660-km Discontinuity Versus Aluminum Content

Aluminum Content, %	Depth Extent of Garnet Below the Discontinuity, km
0	No garnet
1	No garnet
2	No garnet
3	70
4	>100

by 40 km, as double peaks can be observed in the synthetics, different from the seismic data (Figure 15b). Thus the seismic data support the above inference of the properties of phase transformations near the 660-km depth.

7. Comparison to Other Studies

[36] Compared to the studies of the 660-km discontinuity using other approaches, such as precursors to the *PP* and *SS* phases [e.g., Shearer, 1991; Shearer and Flanagan, 1999] or receiver functions [e.g., Niu and Kawakatsu, 1996; Shen et al., 1996], our study can constrain the velocity gradients

above and below the discontinuity, in addition to the velocity jump across the discontinuity and the depth of the discontinuity. The velocity gradient above the 660-km discontinuity is sensitive to mantle temperature and the Al content, and the velocity gradient below the 660-km discontinuity is sensitive to the Al content in the mantle. So these velocity gradients can place significant constraints on mantle temperature and composition. Our study is also affected little by the seismic heterogeneities in the shallower part of the mantle, while the precursor studies and receiver function analyses need to deal with the shallower heterogeneities carefully. Studies using the precursors to the *PP* and *SS* phases, however, provide global coverage of the properties of the 660-km discontinuity and the receiver function studies could provide a better lateral resolution in the study region. The inferred depth of the 660-km discontinuity in our study would also require an accurate determination of event depth.

8. Conclusions

[37] We study seismic *SH* velocity structures, mineralogical models and mantle temperature and composition near the 660-km discontinuity beneath South America and

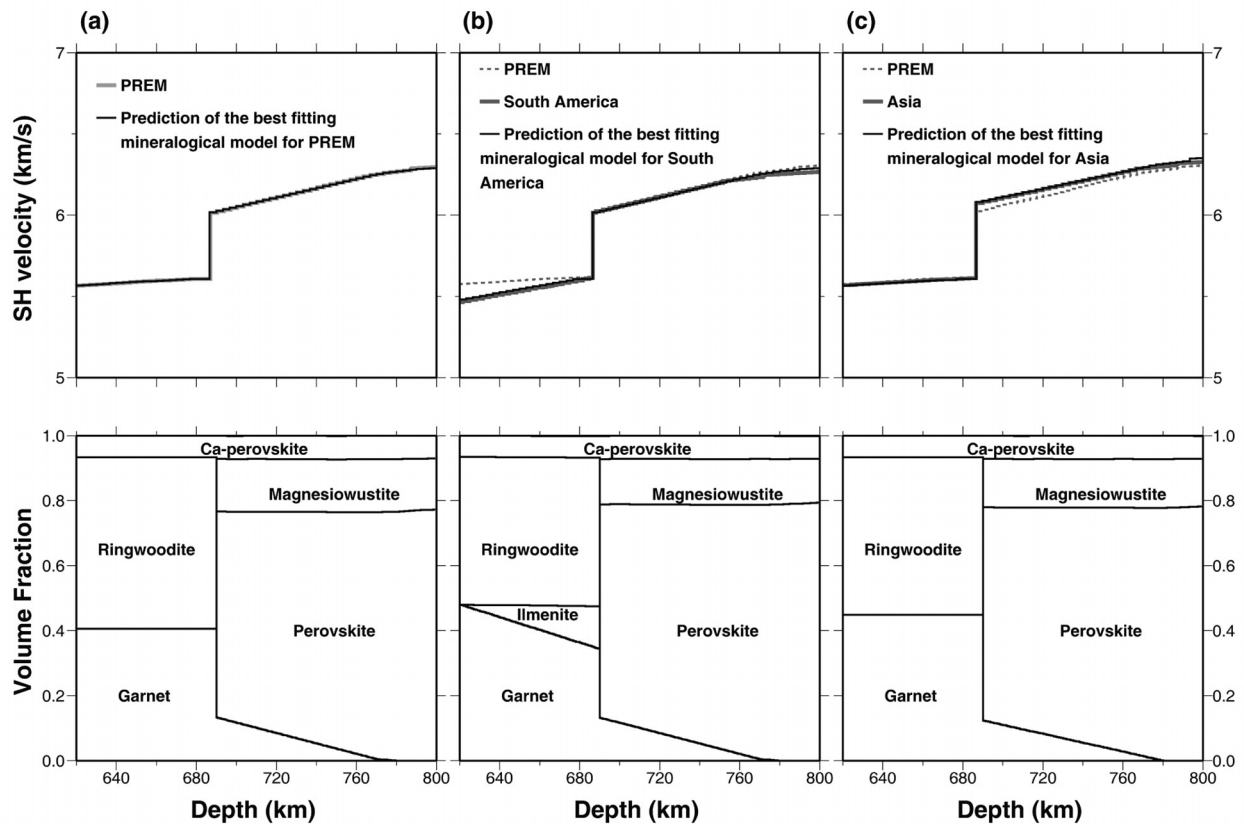


Figure 13. (top) Comparisons between (a) PREM, (b) best fitting model for South America, and (c) best fitting model for northeast Asia, and predicted velocity structures based on three mineralogical models shown in the bottom. Velocity models are calculated on the basis of measured elastic properties, relative volume fractions of these phases, and an adiabatic temperature gradient of 0.7°C/km. PREM is plotted as reference. (bottom) Volume fractions of major mineral phases as a function of depth in three mineralogical models. The phase transformations from ringwoodite to perovskite plus magnesiowustite and from garnet to perovskite are assumed to occur in a same depth in the calculation.

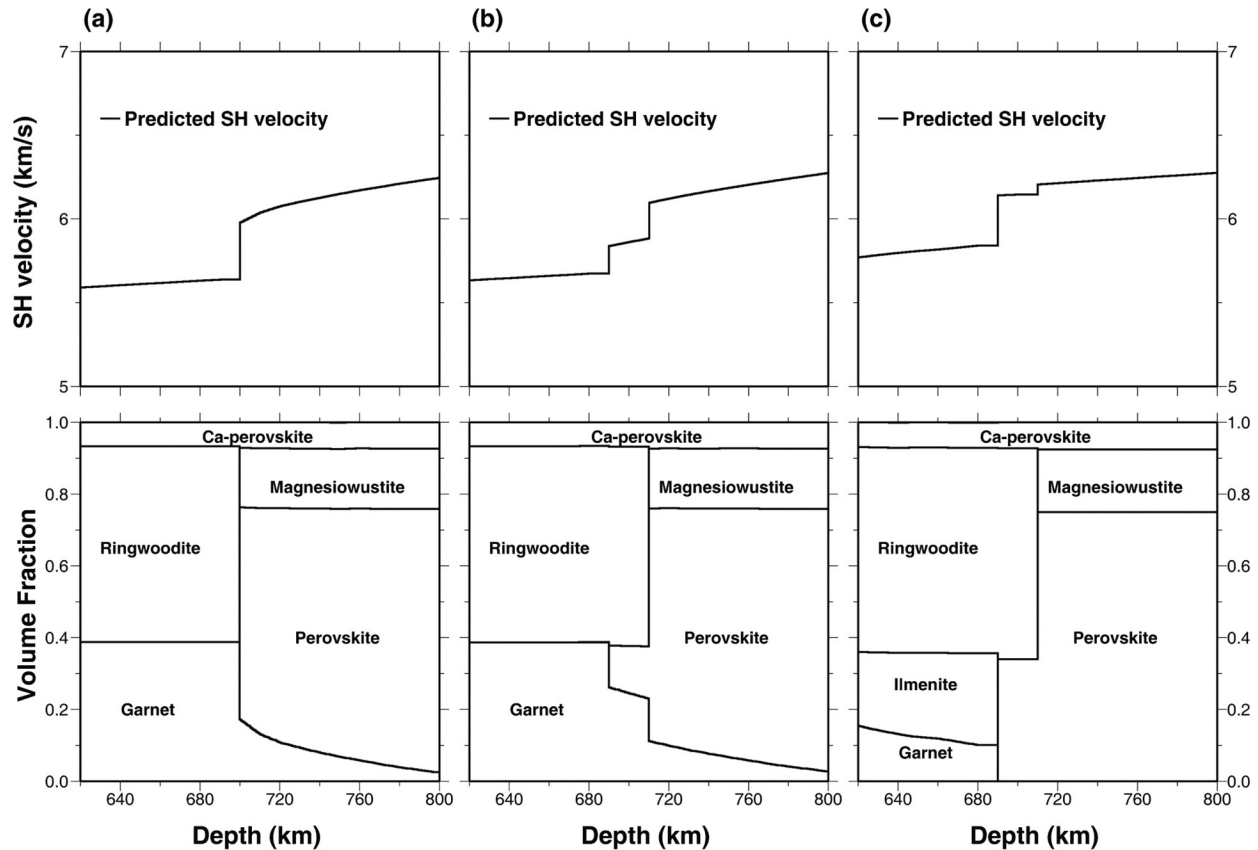


Figure 14. (bottom) volume fractions of major mineral phases as a function of depth for three mantle thermal and compositional models: (a) with a mantle temperature of 1554°C and an Al content of 4%; (b) with a mantle temperature of 1394°C and an Al content of 4%; and (c) with a mantle temperature of 1394°C and an Al content of 1%. (top) SH velocity models predicted based on three mantle thermal and compositional models shown in bottom panels.

northeast Asia, through joint modeling of seismic and mineral physics data. Our seismic data consist of the tangential component of triplicated phases recorded in the epicentral distance range of 10°–35° for a deep event occurring in South America subduction zone and two events occurring in northeast Asia. The data suggest two different SH velocity structures near the 660-km discontinuity beneath South America and northeast Asia. Beneath South America, the velocity gradient above the 660-km discontinuity is larger than that of PREM; while the velocity jump across the discontinuity and the depth extent of the larger velocity gradient below the discontinuity are the same as those of PREM. Beneath northeast Asia, the velocity structures above and below the 660-km discontinuity are the same as that of PREM, while the velocity jump across the discontinuity is larger than that of PREM. The 660-km discontinuity could be double discontinuities with a depth separation less than 20 km, but no more than 40 km.

[38] We infer mantle mineralogical models in the two regions through quantitative comparisons between the seismic models obtained from modeling the seismic data and the velocity structures predicted based on various mineralogical models. In mineral physics modeling, we use phase equilibria data reported in the CaO-MgO- Al_2O_3 - SiO_2

(CMAS) system by Gasparik [1996] to define the stable assemblages at relevant pressures and temperatures, and cation distribution data to define the chemical composition of each phase. This information provides a mineralogical model with volume fractions of each phase. Velocity models are then calculated based on the mineralogical models along with our current estimates of physical properties of the mineral phases.

[39] The different velocity structures in these two regions can be explained by two different mineralogical models. The velocity gradient above the 660-km discontinuity beneath northeast Asia can be explained by temperature and pressure dependencies of the elastic properties of the major phases (ringwoodite + garnet + Ca-perovskite), while the large velocity gradient above the discontinuity beneath South America requires presence of ilmenite. The depth extents of the large velocity gradient below the 660-km discontinuity in the two regions can be explained by the garnet transformation to perovskite persisting to large depths. The larger velocity jump across the discontinuity beneath northeast Asia indicates a larger fraction of garnet transforming to perovskite across the discontinuity than what is required for explaining PREM.

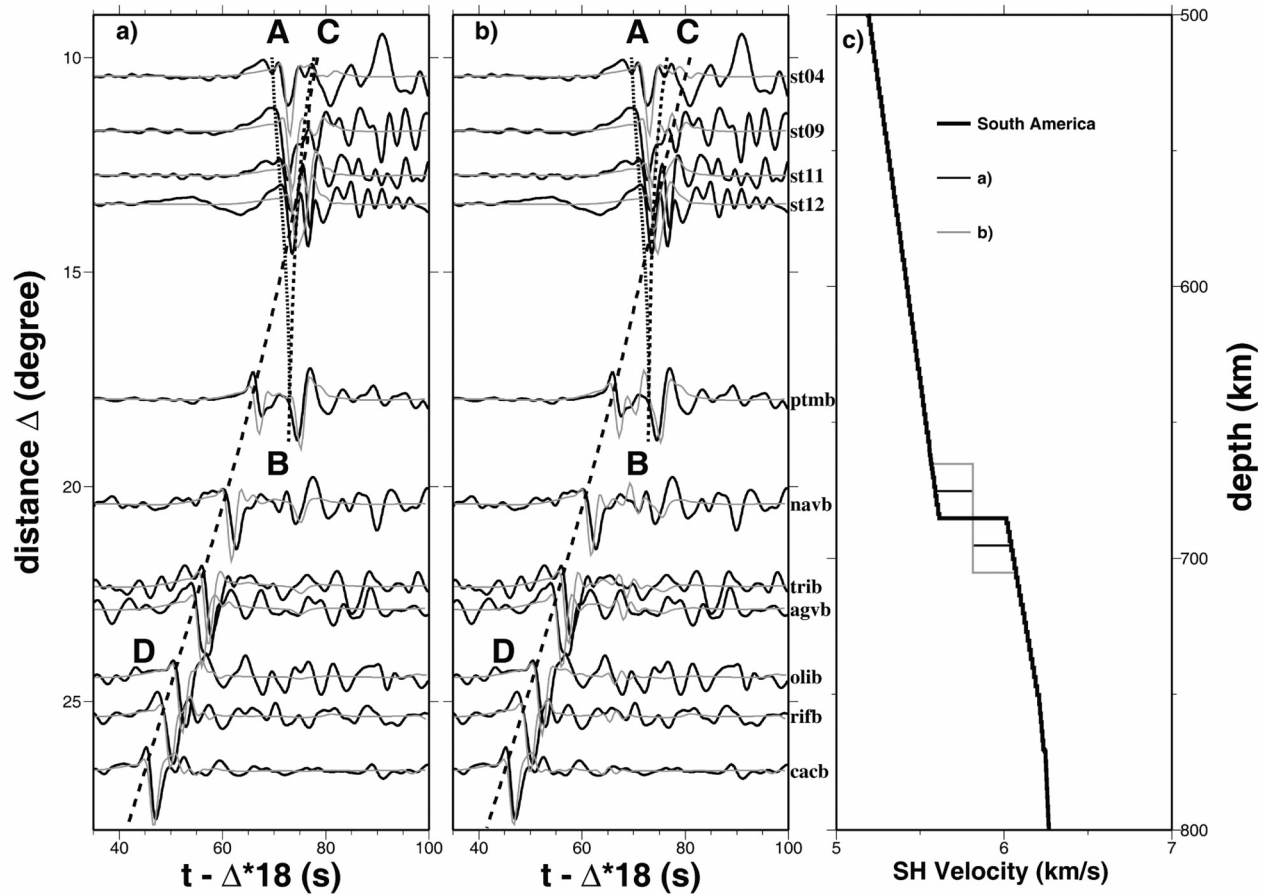


Figure 15. Comparisons of observed tangential displacements for event 1 (black traces) and synthetic waveforms (gray traces) calculated using models perturbed from the best fitting model with double discontinuities near the 600-km depth with depth separations of (a) 20 km and (b) 40 km. (c) Models, labeled accordingly with the synthetics panels.

[40] The depth extent of the large velocity gradient below the 660-km discontinuity can be explained by a lower mantle composition with an aluminum content of 3.4% in the two regions. The different mineralogical models in the transition zone between the two regions can be explained by a difference in mantle temperature and/or composition, especially the aluminum content. Assuming a uniform mantle composition with aluminum of 3.4%, the presence of ilmenite above the 660-km discontinuity beneath South America and the absence of ilmenite beneath northeast Asia would suggest a mantle temperature difference of about 100°C (with that beneath South America being lower) between the two regions. Alternatively, the different mineralogical models above the 660-km discontinuity in these two regions can also be explained by a difference in aluminum content of 1% in mantle composition (with that beneath South America being lower) without invoking a temperature difference between the two regions.

[41] Since at least two phase transformations occur near the 660-km depth and they can interact each other chemically, double discontinuities may exist at the bottom of the transition zone. We discuss the mantle temperature and composition that the double discontinuities may appear, as well as the depth separation and the velocity jumps of the

double discontinuities. For the inferred mantle temperature and composition beneath South America and northeast Asia, the depth separation of double discontinuities is less than 20 km and cannot be resolved by the SH seismic data.

[42] **Acknowledgments.** We thank the principal investigators of the BANJO and BLSP for their efforts in collecting the data and the New Chinese Digital Seismic Network (NCDSN) for providing the data and Baosheng Li, Jennifer Kung, Jihua Chen, an anonymous reviewer and the Associate Editor, Jeroen Ritsema, for reviews. Figures were created with GMT software [Wessel and Smith, 1998]. This work is supported by NSF grant 0439978.

References

- Akaogi, M., and S. Akimoto (1979), High-pressure phase equilibria in a garnet lherzolite, with special reference to Mg^{2+} - Fe^{2+} partitioning among constituent minerals, *Phys. Earth Planet. Inter.*, *19*, 31–51.
- Brudzinski, M. R., and W.-P. Chen (2000), Variations in P wave speeds and outboard earthquakes: Evidence for a petrologic anomaly in the mantle transition zone, *J. Geophys. Res.*, *105*, 21,661–21,682.
- Brudzinski, M. R., and W.-P. Chen (2003), A petrologic anomaly accompanying outboard earthquakes beneath Fiji-Tonga: Corresponding evidence from broadband P and S waveforms, *J. Geophys. Res.*, *108*(B6), 2299, doi:10.1029/2002JB002012.
- Brudzinski, M. R., W.-P. Chen, R. L. Nowack, and B.-S. Huang (1997), Variations of P wave speeds in the mantle transition zone beneath the northern Philippine Sea, *J. Geophys. Res.*, *102*, 11,815–11,827.

- Burdick, L. J., and D. V. Helmberger (1978), The upper mantle P velocity structure of the western United States, *J. Geophys. Res.*, *83*, 1699–1712.
- Chen, W.-P., and M. R. Brudzinski (2003), Seismic anisotropy in the mantle transition zone beneath Fiji-Tonga, *Geophys. Res. Lett.*, *30*(13), 1682, doi:10.1029/2002GL016330.
- Cummins, P. R., B. L. N. Kennett, J. R. Bowman, and M. G. Bostock (1992), The 520-km discontinuity, *Bull. Seismol. Soc. Am.*, *82*, 323–336.
- Dziewonski, A. M., and D. L. Anderson (1981), Preliminary reference Earth model, *Phys. Earth Planet. Inter.*, *25*, 297–356.
- Gasparik, T. (1990), Phase relations in the transition zone, *J. Geophys. Res.*, *95*, 15,751–15,769.
- Gasparik, T. (1996), Melting experiments on the enstatite-diopside join at 70–224 kbar, including the melting of diopside, *Contrib. Mineral. Petrol.*, *124*, 139–153.
- Given, J. W., and D. V. Helmberger (1980), Upper mantle structure of northwestern Eurasia, *J. Geophys. Res.*, *85*, 7183–7194.
- Grand, S. P., and D. V. Helmberger (1984a), Upper mantle shear structure of North America, *Geophys. J. R. Astron. Soc.*, *76*, 399–438.
- Grand, S. P., and D. V. Helmberger (1984b), Upper mantle shear structure beneath the northwest Atlantic Ocean, *J. Geophys. Res.*, *89*, 11,465–11,475.
- Hager, B. H. (1984), Subducted slabs and the geoid: Constraints on mantle rheology and flow, *J. Geophys. Res.*, *89*, 6003–6015.
- Helmberger, D. V., and R. A. Wiggins (1971), Upper mantle structure of midwestern United States, *J. Geophys. Res.*, *76*, 3229–3245.
- Honda, S., and D. R. S. Balachandar (1993), Three-dimensional mantle dynamics with an endothermic phase transition, *Geophys. Res. Lett.*, *20*, 221–224.
- Irifune, T., and A. E. Ringwood (1987), Phase transformations in primitive morib and pyrolite compositions to 25 gpa and some geophysical implications, in *High Pressure Research in Geophysics*, edited by M. H. Manghnani and Y. Syono, pp. 231–242, AGU, Washington, D. C.
- Ito, E., and E. Takahashi (1987), Ultrahigh-pressure phase transformations and the constitution of the deep mantle, in *High Pressure Research in Geophysics*, edited by M. H. Manghnani and Y. Syono, pp. 221–229, AGU, Washington, D. C.
- LeFevre, L. V., and D. V. Helmberger (1989), Upper mantle P velocity structure of the Canadian shield, *J. Geophys. Res.*, *94*, 17,749–17,765.
- Melbourne, T., and D. V. Helmberger (1998), Fine structure of 410 km discontinuity, *J. Geophys. Res.*, *103*, 10,091–10,102.
- Morgan, J. P., and P. M. Shearer (1993), Seismic constraints on the mantle flow and topography of the 660-km discontinuity: Evidence for whole mantle convection, *Nature*, *365*, 506–511.
- Neele, F. (1996), Sharp 400-km discontinuity from short-period P reflections, *Geophys. Res. Lett.*, *23*, 419–422.
- Niu, F., and H. Kawakatsu (1996), Complex structure of mantle discontinuities at the tip of the subducting slab beneath Northeast China—A preliminary investigation of broadband receiver functions, *J. Phys. Earth*, *44*, 701–711.
- Richards, M. A., and B. H. Hager (1984), Geoid anomalies in a dynamic Earth, *J. Geophys. Res.*, *89*, 5987–6002.
- Shearer, P. M. (1991), Constraints on upper mantle discontinuities from observations of long-period reflected and converted phases, *J. Geophys. Res.*, *96*, 18,147–18,182.
- Shearer, P. M., and M. P. Flanagan (1999), Seismic velocity and density jumps across the 410- and 660-kilometer discontinuities, *Science*, *285*, 1545–1548.
- Shen, Y., S. C. Solomon, I. T. Bjarnason, and G. M. Purdy (1996), Hot mantle transition zone beneath Iceland and the adjacent Mid-Atlantic Ridge inferred from P-to-S conversions at the 410- and 660-km discontinuities, *Geophys. Res. Lett.*, *23*, 3527–3530.
- Song, T. A., D. V. Helmberger, and S. P. Grand (2004), Low-velocity zone atop the 410-km seismic discontinuity in the northwestern United States, *Nature*, *427*, 530–533.
- Tackley, P. J., D. J. Stevenson, G. A. Glatzmaier, and G. Schubert (1993), Effects of an endothermic phase transition at 670 km depth in a spherical model of convection in the Earth's mantle, *Nature*, *361*, 699–703.
- Walck, M. C. (1984), The P-wave upper mantle structure beneath an active spreading centre: The Gulf of California, *Geophys. J. R. Astron. Soc.*, *76*, 697–723.
- Weidner, D. J., and Y. Wang (1998), Chemical and Clapeyron induced buoyancy at the 660 km discontinuity, *J. Geophys. Res.*, *103*, 7431–7441.
- Weidner, D. J., and Y. Wang (2000), Phase transformations: Implications for mantle structure, in *Earth's Deep Interior: Mineral Physics and Tomography From the Atomic to the Global Scale*, *Geophys. Monogr. Ser.*, vol. 117, edited by S.-I. Karato, A. M. Forte, R. C. Liebermann, G. Masters, and L. Stixrude, pp. 215–235, AGU, Washington, D. C.
- Wen, L., and D. L. Anderson (1997a), Layered mantle convection: A model for geoid and topography, *Earth Planet. Sci. Lett.*, *146*, 367–377.
- Wen, L., and D. L. Anderson (1997b), Present-day plate motion constraint on mantle rheology and convection, *J. Geophys. Res.*, *102*, 24,639–24,654.
- Wessel, P., and W. H. F. Smith (1998), New, improved version of Generic Mapping Tools released, *Eos Trans. AGU*, *97*, 597.
- Zhao, M., C. A. Langston, A. A. Nyblade, and T. J. Owens (1999), Upper mantle velocity structure beneath southern Africa from modeling regional seismic data, *J. Geophys. Res.*, *104*, 4783–4794.
- Zhu, L. P., and L. A. Rivera (2002), A note on the dynamic and static displacements from a point source in multilayered media, *Geophys. J. Int.*, *148*, 619–627.

Y. He, Institute of Geology and Geophysics, Chinese Academy of Sciences, Beijing, China. (ymhe@mail.iggcas.ac.cn)

Y. Wang, D. Weidner, and L. Wen, Department of Geosciences, State University of New York at Stony Brook, Stony Brook, NY 11794, USA. (yiwang@mantle.geo.sunysb.edu; dweidner@notes.cc.sunysb.edu; lianxing.wen@sunysb.edu)